A R C H I V E S O F M E T A L L U R G Y A N D M A T E R I A L S
Volume 60 2015 Issue 3
DOI: 10.1515/amm-2015-0380

W. BOCHNOWSKI*#, A. DZIEDZIC*, S. ADAMIAK*, M. BERCHENKO**, M. TRZYNA**, J. CEBULSKI*

CHARACTERIZATION OF OXIDE LAYERS PRODUCED ON THE AISI 321 STAINLESS STEEL AFTER ANNEALING

CHARAKTERYSTYKA WARSTW TLENKOWYCH POWSTAŁYCH NA STALI NIERDZEWNEJ AISI 321 PO WYŻARZANIU

In this study, the structure, chemical composition and topography of oxide layers produced on the surface of the AISI 321 austenitic steel in the annealing process were analyzed. Heat treatment was done at 980°C temperature for 1 hour time in different conditions. The annealing was done in a ceramic furnace in oxidation atmosphere and in vacuum furnaces with cylindrical molybdenum and graphite chambers. The analysis was carried out using the following methods: a scanning electron microscope (SEM) equipped with an energy-dispersive X-ray spectrometer (EDX), a transmission electron microscope (TEM) equipped with an energy-dispersive X-ray spectrometer (EDX), an X-ray diffractometer (XRD), a secondary ion mass spectrometer with time-of-flight mass analyzer (TOF SIMS) and an atomic force microscope (AFM). The oxide layer formed during annealing of the AISI 321 steel at 980°C consisted of sub-layers, diversified in the chemical composition. The thickness of the oxidized layer is depended on the annealing conditions. In a ceramic furnace in oxidation atmosphere, the thickness of the oxide layer was of 300-500 nm, in a vacuum furnace with molybdenum and graphite heating chambers, it ranged from 40 to 300 nm and from a few to 50 nm, respectively. TOF SIMS method allows to get average (for the surface of 100 μm × 100 μm) depth profiles of concentration of particular elements and elements combined with oxygen. In oxide layers formed in vacuum furnaces there are no iron oxides. Titanium, apart from being bounded with carbon in carbides, is a component of the oxide layer formed on the surface of the AISI 321 steel.

Keywords: depth profile, oxide layer, stainless steel, TEM, TOF SIMS

W pracy analizowano strukturę, skład chemiczny oraz topografię warstwy tlenków powstałych na powierzchni stali austenitycznej AISI 321 w procesie wyżarzania. Obróbkę cieplną prowadzono w temperaturze 980°C w czasie 1 godziny w zróżnicowanych warunkach. Wyżarzanie prowadzono w piecu ceramicznym w atmosferze powietrza oraz w piecach próżniowych z cylindryczną komorą molibdenową i grafitową. W prowadzonej analizie wykorzystano skaningowy mikroskop elektronowy (SEM) wyposażony w spektrometr promieniowania X (EDX), transmisyjny mikroskop elektronowy (TEM) wyposażony w spektrometr promieniowania X (EDX), dyfraktometr rentgenowski (XRD X-Ray Diffraction), spektrometr mas jonów wtórnych z analizatorem czasu przelotu (TOF SIMS) oraz mikroskop sił atomowych (AFM). Warstwa tlenków powstała w wyniku wyżarzania stali AISI 321 w temperaturze 980°C składała się z podwarstw różniących się składem chemicznym. O grubości warstwy utlenionej w decydowały warunki wyżarzania. W piecu ceramicznym z atmosferą powietrza grubość warstwy tlenków wynosiła 300-500 μm, w piecu próżniowym z grafitową i molibdenową komorą grzejną grubości wynosiły odpowiednio od 40 nm do 300 nm oraz kilka nm do 50 nm.

Badania TOF SIMS pozwalają otrzymać uśrednione profile koncentracji pierwiastków metalicznych oraz profile koncentracji pierwiastków metalicznych będących w kontakcie z tlenem. W warstwach tlenków powstałych w piecach próżniowych nie obserwowano tlenków żelaza. Tytan oprócz roli związania węgla w węglikach, wchodzi w skład warstwy tlenków tworzonych w piecu próżniowym na powierzchni stali AISI 321.

1. Introduction

Austenitic stainless steels are widely used in automobile, aviation, chemical and food industries [1,2]. Adding 18% chromium and 9% nickel to steel containing less than 0,1% carbon ensures austenitic structure needed for high resistance to corrosion. In temperatures above 550°C carbon diffusion to grain boundaries occurs in steel. As a result of carbon diffusion, chromium carbides appear at austenite grain boundaries, the chromium content on the boundary is decreasing below about

* CENTER FOR INNOVATION AND TRANSFER OF NATURAL SCIENCES AND ENGINEERING KNOWLEDGE, UNIVERSITY OF RZESZOW, 1 PIGONIA STR., 35-959 RZESZOW, POLAND.
** CENTER FOR MICROELECTRONICS & NANOTECHNOLOGY, UNIVERSITY OF RZESZOW, 1 PIGONIA STR., 35-959 RZESZOW, POLAND.
# Coresponding author: wobochno@univ.rzeszow.pl

12%, causing intercrystalline corrosion. To prevent intercrystalline corrosion, titanium is added to steel. Titanium is bounded with carbon in carbides, which will become stable in increased temperature [3]. According to [4] the high corrosion resistance in stainless steel can be achieved by formation of Cr_2O_3 layer. Annealing is used to improve the corrosion resistance of stainless steels. During the heat treatment at high temperatures, oxidation of the surface of stainless steels occurs. The oxidation of surface of stainless steels also occurs at high temperatures during the processes of plastic forming, heat treatment while laser cutting and welding of steel elements. [5,6,7]. To improve the corrosion resistance of the AISI 321 stainless steel, annealing in 950-1100°C temperatures with intensive cooling is applied [8]. Predominantly the heat treatment is done in vacuum furnaces which prevents the formation of oxide layer (several dozen micrometers thick) on the surface of stainless steel. When heat treatments are done in an oxidizing atmosphere the oxide should be removed after annealing in a descaling solution such as a mixture of nitric and hydrofluoric acids. In industry, horizontal loaded, electric vacuum furnaces (10^{-4} Pa) with cylindrical molybdenum or graphite chambers are used. After heat treatment in a vacuum furnace, an oxide layer, several dozen nanometers thick, is formed on the surface of steel. One of the techniques of joining stainless steels frequently used in automobile and aviation industries is brazing. Too thick oxide layer produced during heat treatment of stainless steel can make brazing of stainless steels impossible [9]. The native oxide layer on stainless steel is usually 1-3 nm thick. The oxide layer's structure affects reactivity, adhesion to the surface and therefore the corrosion resistance. There are few analytical studies on oxide layers in nano-scale [10,11]. The previous studies explaining the mechanism of oxidation were based on the oxidation of FeCrNi single crystals [12]. The authors of the article [10] showed that after placement the stainless steel into a pressure chamber containing 99% oxygen at 10^{-5} mbar, after 10 minutes an oxide layer 3 nm thick is formed on the surface of steel. Thicker (a few micrometers) oxide layer has influence on the mechanical parameters of stainless steel in elevated temperatures [13]. There is no publications on the analysis of the oxides layers on the AISI 321 steel, which were created after heat treatment in the industrial vacuum furnaces. It is extremely important to know about the thickness, morphology and the order of formation of oxides during heat treatment of stainless steels. The work describes structural changes in oxide layers produced during heat treatment on the surface of the AISI 321 stainless steel. Using such research devices as SEM, AFM, XRD, TOF SIMS, TEM and EDX allowed to analyze structural changes in micro- and nano-oxidized layer.

2. Material and experimental procedures

Plates of the AISI 321 stainless steel were analyzed in this study. The plates were of 25×10×1 mm size. The chemical composition of the investigated material determined by Spark spectrometer Solaris CCD Plus, is shown in Table 1.

TABLE 1

The chemical composition of the AISI 321 steel

Element	C	Mn	Si	P	S	Cr	Ni	Ti
Content wt.%	0.06	2.01	0.54	0.03	0.02	17.9	8.54	0.14
Element	**Nb**	**V**	**Mo**	**Co**	**W**	**Al**	**Cu**	**Fe**
Content wt.%	0.05	0.12	0.30	0.16	0.04	0.05	0.42	balance

The as-received samples were annealed for 30 minutes at 1050°C. The sample surface was polished with an emery paper (2000), then with 0.3 μm grade aluminum oxide and then cleaned with ethanol. Next, the samples were annealed for 60 minutes at 980°C. This procedure resulted in maximum ductility. The annealing process was conducted in three different industrial resistance furnaces. The ceramic furnace with oxidation atmosphere (NABERTHERM gmbh HT04/16) and horizontal vacuum furnace (HVF) with cylindrical molybdenum and cylindrical graphite chambers, respectively, were used. In each of the vacuum furnaces there was a working chamber of 900×600×1600 mm, with the temperature tolerance of ±10°C for the temperature tested. The annealing in vacuum furnaces was done under 10^{-5} Pa pressure. After annealing the samples were cooled in argon beam. Structure characterization of the material was carried out with a SEM FEI Quanta 3D 200i using an EDAX Ametek energy-dispersive spectrometer (EDS). The nano-scale microstructure observations and the chemical composition measurements were performed by means of TEM using a FEI Tecnai Osiris microscope (200 kV). The TEM was equipped with a field emission gun and a high angle annular dark field scanning/transmission detector HAADF/STEM combined with an energy dispersive spectrometer EDS. To prepare the thin lamella for the TEM test (Fig. 1), Focused Ion Beam (FIB) method was used.

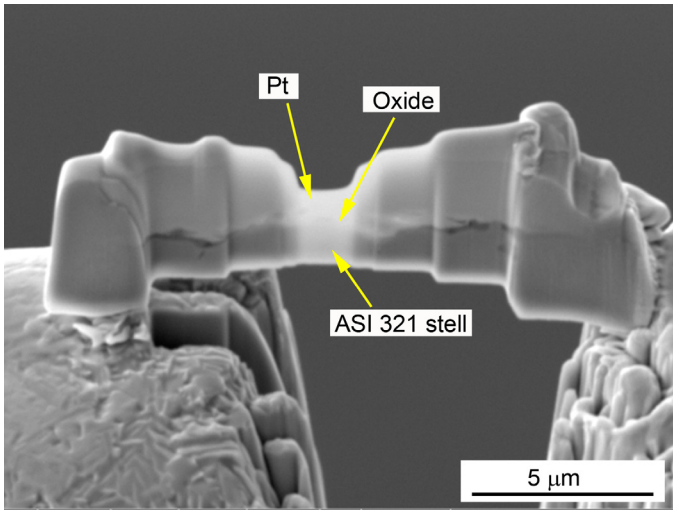

Fig. 1. The thinned lamella prepared for TEM test

X-ray diffraction patterns were taken immediately from the surface of the plate specimens on a Bruker D8 Apparatus using Cu *Kα* radiation with Bruker EVA software. Time-of-flight secondary

ion mass spectrometry data were acquired using a TOF-SIMS V spectrometer (ION-TOF GmbH, Muenster, Germany). The analysis chamber was maintained at less than 5×10^{-9} Pa under operational conditions. A pulsed 30 keV Bi^+ primary ion source at a current of 1.3 pA (high current bunched mode), rastered over a scan area of 100 µm×100 µm was used as the analysis beam. TOF-SIMS depth profiles were measured with the instrument working in the dual-beam mode. The sputtering was performed using a 2 keV (100 nA) Cs^+ ion beam. Both ion beams were impacting the sample surface at the 45° angle to the normal and ions were collected from the center of the sputtered crater. The sputtering rate of oxide was established by combining a series of external measurements of crater depths, performed by a mechanical profilometer, after depth profiling for a certain time, in the same energy and current conditions. Atomic Force Microscope (AFM) imaging in non-contact mode was performed in air, at room temperature using the AFM from CSM Instruments.

3. Results and discussion

3.1. Tests results of the microstructure and chemical composition (SEM with EDS, XRD, AFM)

The XRD results of the surface of the AISI 321 stainless steel before oxidation indicated the presence of austenite γ and phase α' (Fig. 2).

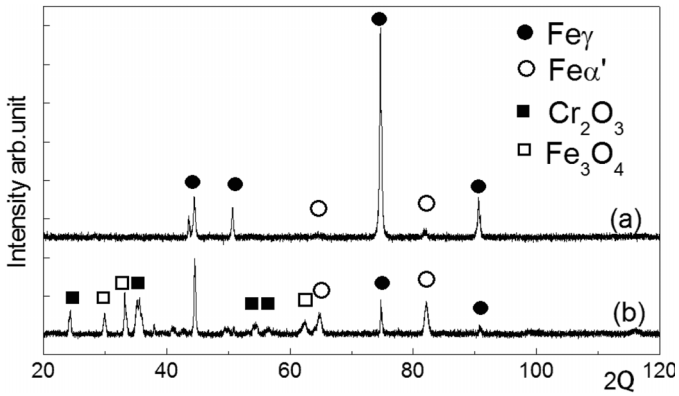

Fig. 2. The XRD patterns of oxidation layer of the AISI 321 steel as-received (a) and after annealing in a ceramic furnace oxidation atmosphere (b)

Fig. 3. shows structure profiles of the AISI 321 steel as-received and after annealing in different furnaces. The AFM measurements proved that an average roughness of the surface of the AISI 321 stainless steel before oxidation, measured on the surface of 10×10 µm was Ra = 1,5 nm.

After annealing of the AISI 321 steel in a ceramic furnace in oxidation atmosphere, the porous oxide layer, 300-500 µm thick, was formed on the surface of steel. The oxide layer has diverse chemical composition and morphology (Fig. 4,5) on cross-section. Chemical composition results obtained using SEM with EDX and XRD show that the oxide layer, from the surface side, was mainly composed of Cr_2O_3 and Fe_3O_4. It is generally agreed that the oxide films are formed by diffusion of Fe to the outer oxide layer [14]. The analysis of EDS chemical composition revealed diversified stratification of oxides. From the surface side of the oxide layer, the Fe, Si, Al rich sub-layer was formed. Below the sub-layer of oxides consists of Cr, Ni, Mn and Ti.

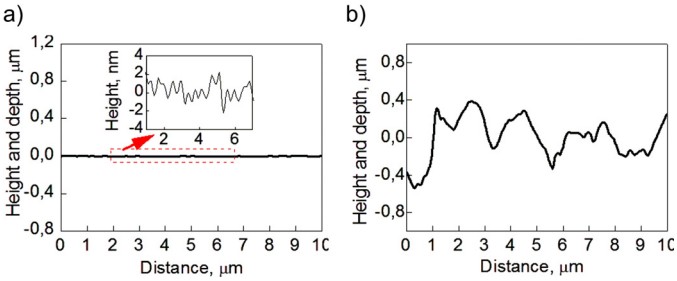

Fig. 3. The surface profiles of oxide layer of the AISI 321 steel as-received (a) and after annealing in a ceramic furnace oxidation atmosphere (b)

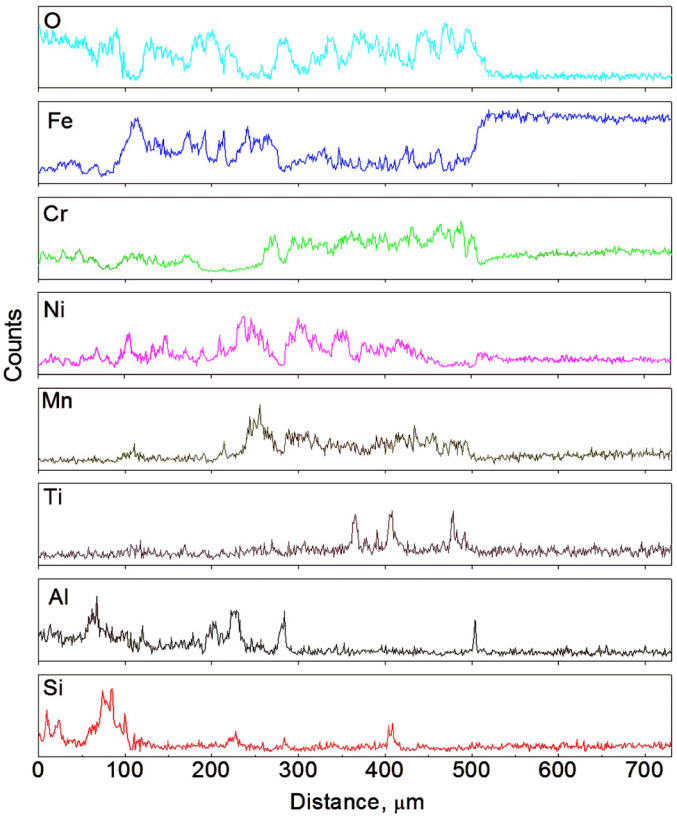

Fig. 4. EDS chemical composition change along the indicated A line on the Fig. 5b

On the cross-section of oxide layer the spinel crystals about 2 µm and crystals smaller than 1 µm in groups forming spheres could be observed. The spinel crystals (of 1 to 4 µm) contained more Fe and Ni and less O, Mn and Cr in comparison to crystals situated in groups forming spheres (Fig. 5c). The spheres were smaller than 10 µm. The similar spinels forming spheres in the oxidized layer on ferrite steel were observed by [15]. The authors,

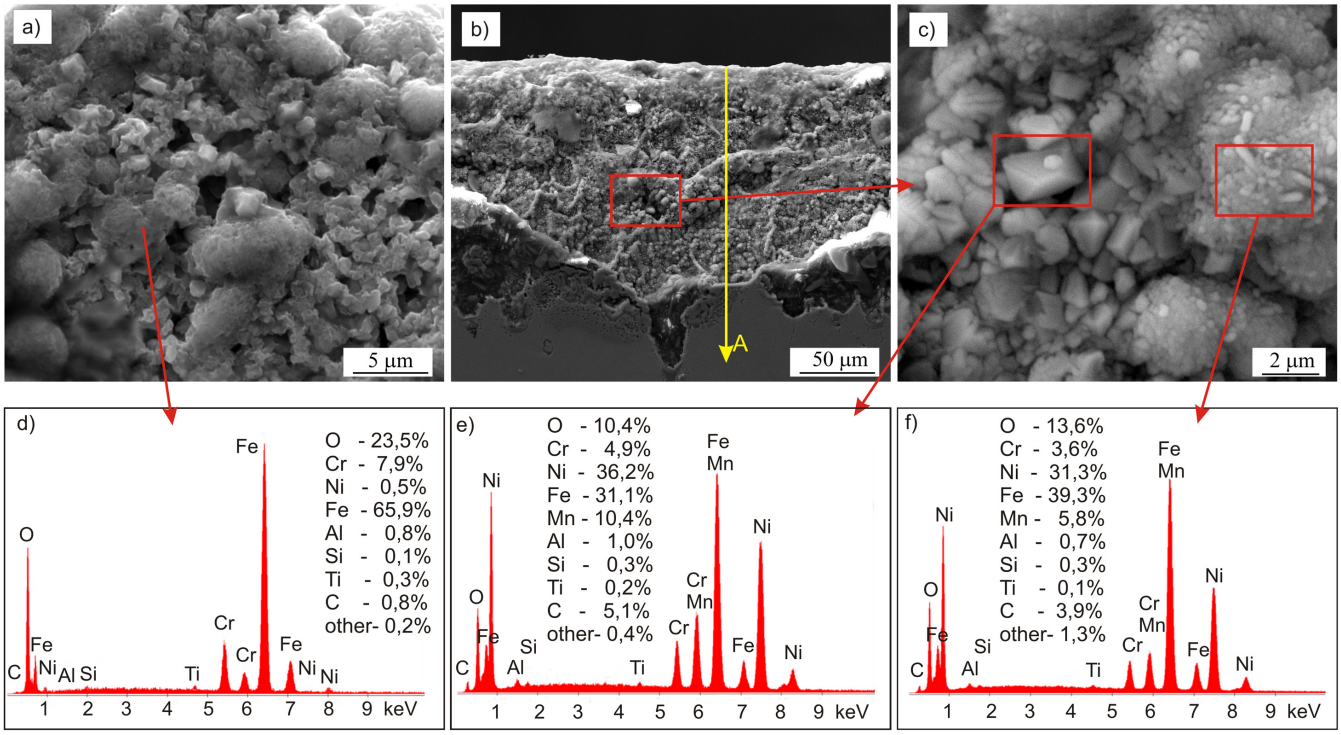

Fig. 5. The microstructure of the oxidized layer of the AISI 321 steel as a result of annealing in a ceramic furnace in oxidation atmosphere: a) the surface of the oxidized layer, b) cross-section of the oxidized layer, c) microstructure in Fig. b. enlargement, d) EDS spectrum and chemical composition (wt.%) of the surface in Fig. a, e-f) EDS spectrum, point analysis of the chemical composition (wt.%) for the areas in Fig. c

taking into consideration of the increased content of Cr, Mn and O defined the spinels as $MnCr_2O_4$. The observed oxide layer was formed by diffusion of metal ions and diffusion of external oxygen molecules inside the material. The porous oxide layer allows oxygen molecules to move into the oxidized layer. The oxides being formed inside the oxidized layer (Fig. 5) contain more Ni and Mn and less Cr and Fe in comparison to the oxides on the surface of the oxidized layer. In the XRD patterns of the AISI 321 steel after annealing in a ceramic furnace in oxidation atmosphere apart from oxide phases, austenite peaks from fcc phase and ferrite peaks from bcc phase could be identified (Fig. 2). The presence of ferrite is the result of the surface layer of steel depleted of chromium. Chromium and iron were the basic elements forming oxides. The austenite depleted of chromium transforms to austenite γ and phase α'. The measurements of AFM topography showed that average roughness measured on the surface of 10 µm×10 µm was Ra = 298 nm (Fig. 3). After annealing of the AISI 321 steel in a vacuum furnace with cylindrical graphite chamber, on the surface of steel the oxide layer of grain structure was formed. The average size of a grain was approximately of 5 µm (Fig. 6). SEM with EDS chemical composition results showed lower oxygen content 14.50 wt.% in the oxidized layer in comparison to the oxidized layer formed in a ceramic furnace in oxidation atmosphere (23.50 wt.%). AFM measurements proved that average roughness of the sample measured on the surface of 10 µm×10 µm was Ra = 143 nm (Fig. 6).

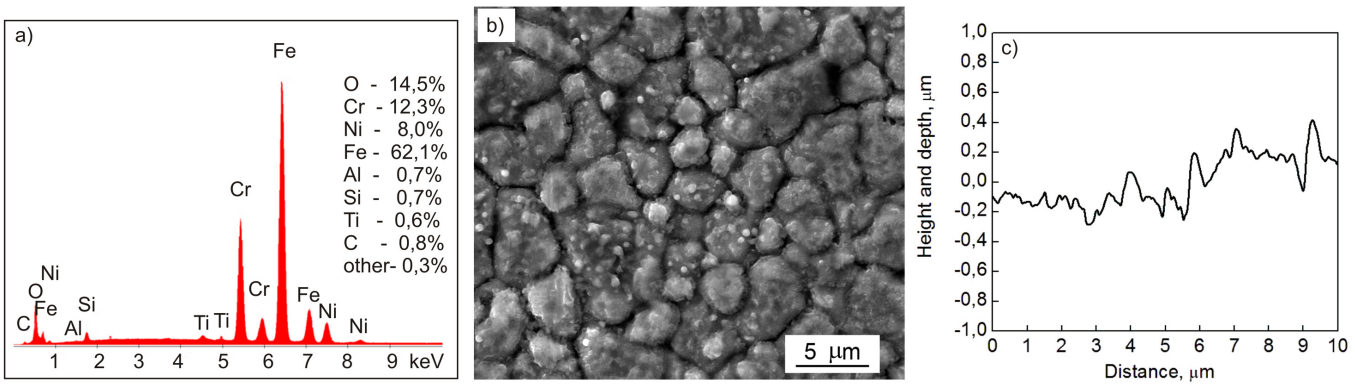

Fig. 6. The microstructure of the oxidized layer of the AISI 321 steel as a result of annealing in a vacuum furnace with cylindrical graphite chamber: a) EDS spectrum and chemical composition (wt.%) of the surface in Fig. b, b) microstructure of the surface of oxides, c) profiles of the oxide layer surface

After annealing of the AISI 321 steel in a vacuum furnace with cylindrical molybdenum chamber, on the surface of steel the oxide layer of grain structure was formed. The average size of a grain was approximately of 8 μm (Fig. 7). SEM with EDS chemical composition results showed the lowest oxygen content 2,8 wt.% in the oxidized layer. AFM measurements proved that an average roughness of the sample measured on the surface of 10 μm×10 μm was Ra = 98 nm. In case of annealing in vacuum furnaces with cylindrical molybdenum and graphite chambers, there appear wide (0.2 μm) boundaries between grains forming the oxidized layer, which can make the diffusion of oxygen molecules to the surface of steel possible.

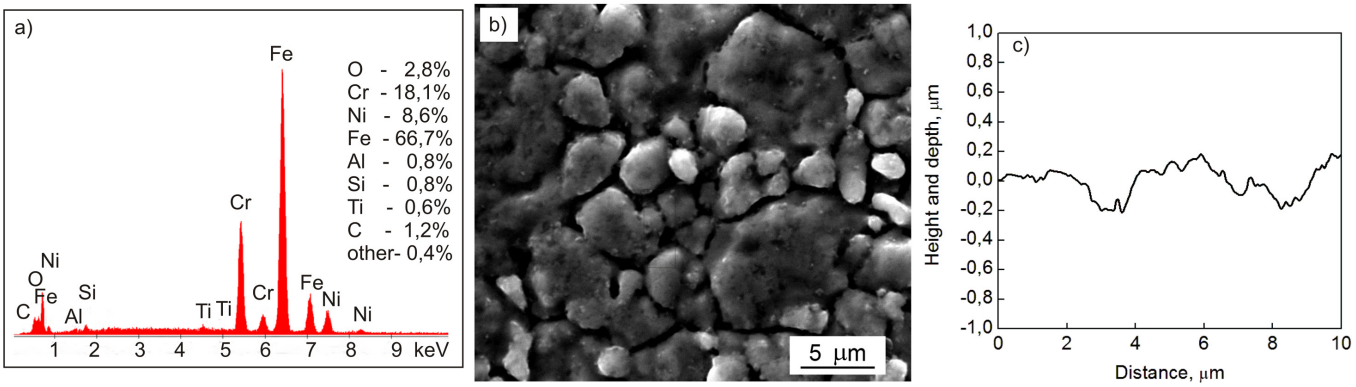

Fig. 7. The microstructure of the oxidized layer of the AISI 321 steel as a result of annealing in a vacuum furnace with molybdenum heating chamber: a) EDS spectrum and chemical composition (wt.%) of the surface in Fig. b., b) microstructure of the surface of oxides, c) profiles of the oxide layer surface

3.2. Structural changes analyzed by TEM/EDS system

Using the TEM equipped with a HAADF/STEM detector on cross-section allowed to indicate that the AISI 321 steel after annealing in a vacuum furnace with cylindrical graphite chamber had diverse thickness of the oxidized layer, ranging from 40 to 300 nm (Fig. 8). The oxidized layer was the thickest at the boundaries of oxide grains. The surface analysis of the EDS chemical composition revealed sub-layer structure of the oxidized layer. In the oxidized layer an increase of concentration of Mn and Cr could be observed. At the bottom of the oxidized layer (at the surface of the steel) an increase of concentration of Ti and V and the Si-rich areas of 30-50 nm size could be observed. Silicon oxide in the oxides layer on the 316 steel were also observed in [16]. The analysis of the EDS chemical composition carried out at the lowest thickness of the oxide layer and

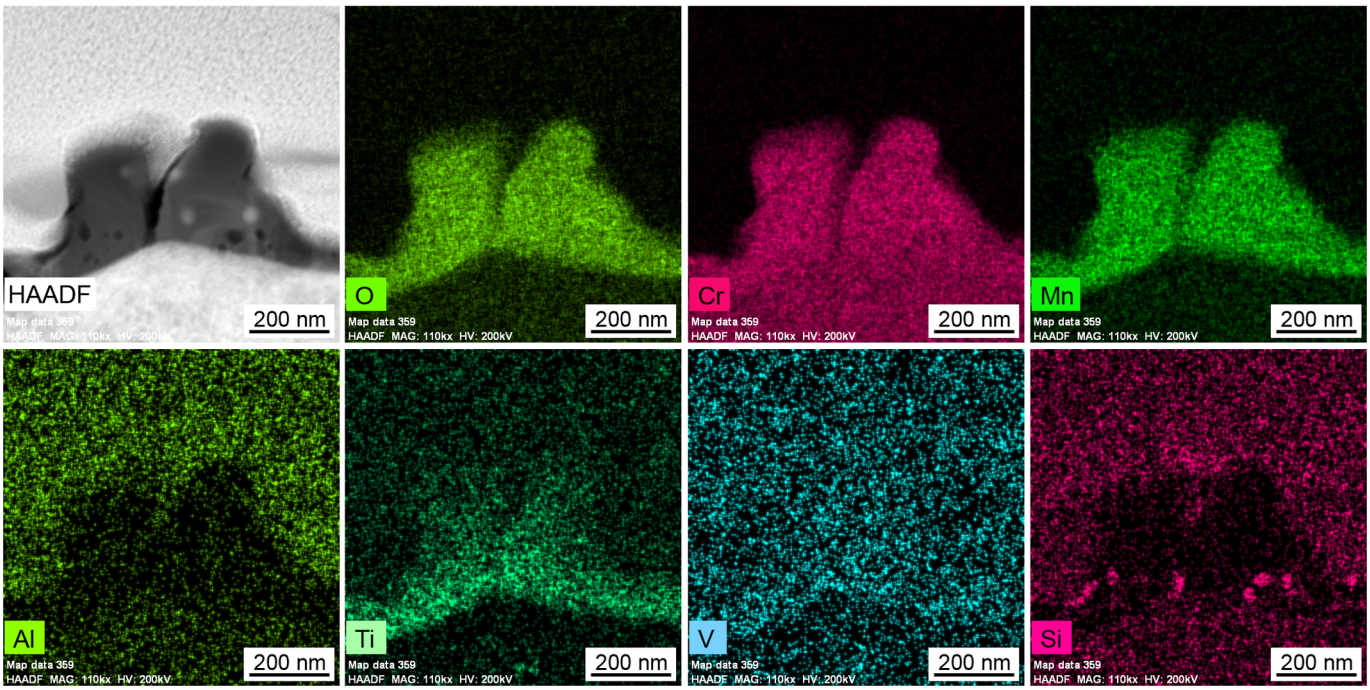

Fig. 8. The maps of TEM with EDS chemical composition on cross-section of the oxidized layer formed on the AISI 321 steel in a vacuum furnace with graphite heating chamber

along the line at the highest thickness of the oxide layer proves the sub-layer structure (Fig. 9). The sub-layer structure of the oxidized layer of the AISI 316 stainless steel was also obtained by the authors [17].

The oxidized layer of the lowest thickness ranging from a few to 50 nm was obtained after heat treatment done in a vacuum furnace with cylindrical molybdenum chamber (Fig. 10, 11). The oxides did not form a firm layer, they occurred in groups. The surface and line analysis of EDS chemical composition revealed diversified stratification of oxide layer. On the cross-section, the areas of several dozen nanometers of various concentration of elements could be noticed. At the top of the oxidized layer (at the surface) there was an increase of Al concentration, at the bottom an increase of concentration of Cr, Mn, Ti and V could be observed. In oxide layer which produces in the vacuum furnaces the spinel crystals were not observed.

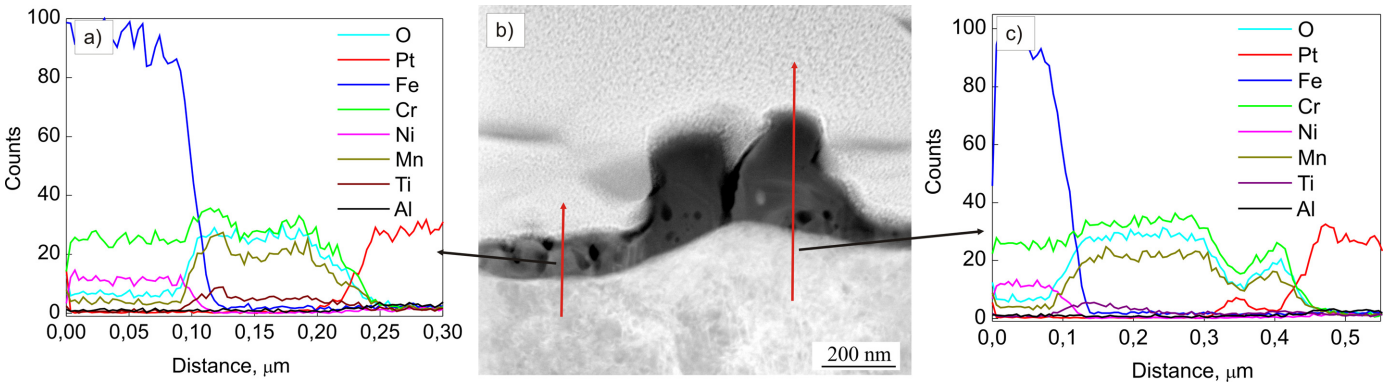

Fig. 9. The HAADF/STEM image presenting the structure of oxides and the analysis of TEM with EDS chemical composition on cross-section of the oxidized layer formed on the AISI 321 steel in a vacuum furnace with graphite heating chamber

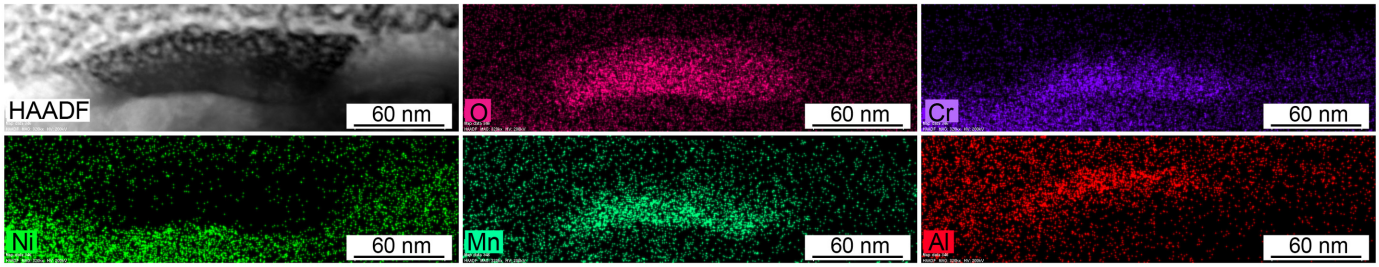

Fig. 10. The maps of TEM with EDS chemical composition on cross-section of the oxidized layer formed on the AISI 321 steel in vacuum furnace with molybdenum heating chamber

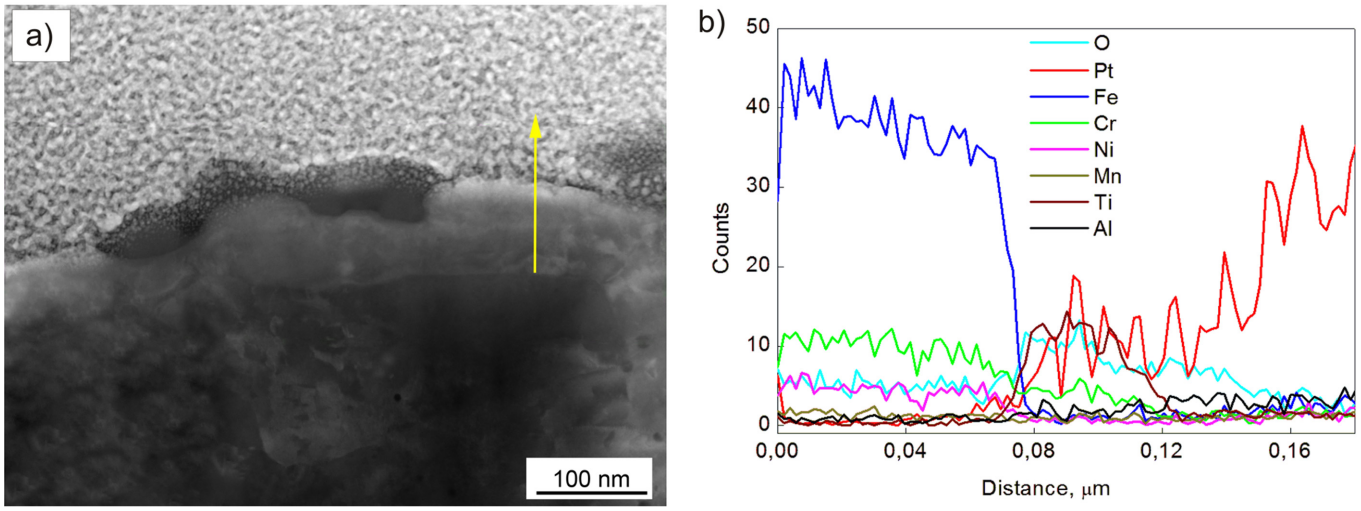

Fig. 11. The HAADF/STEM image presenting the structure of oxides and the analysis of TEM (a); EDS chemical composition on the cross-section of the oxidized layer formed on the AISI 321 steel in a vacuum furnace with molybdenum heating chamber (b)

3.3. Change of the chemical concentration analyzed by TOF SIMS

The experimental method used allows to get average (for the surface of 100 μm×100 μm) profiles of concentration of particular elements and elements connected with oxygen. Fig. 12 shows TOF SIMS results concerning the oxide layer formed on the AISI 321 steel in a vacuum furnace with graphite and molybdenum heating chamber, respectively.

The etching time during TOF SIMS examination was 5500 s. After 1500 s. and 400 s. appropriately for samples annealed in a vacuum furnace with graphite chamber and samples annealed in a vacuum furnace molybdenum chamber, the stable concentration of the analyzed metallic elements could be noticed. The graphs present different profile patterns of concentration of elements depending on the conditions of annealing. Fig. 12ab. (for the oxide layer formed during annealing in a graphite chamber) shows the proportional increase of Fe, Ni, Cr concentration and decrease in concentration of oxygen during etching. Fig. 12a,b also indicates that after 300 s. of etching, the stabilization of oxygen concentration takes place which means that it reached the surface of steel. Further etching showed that directly below the oxide layer of the stainless steel there was a decrease of Fe, Ni and Cr concentration. This decrease is the result of core material diffusion of these elements from the steel to the oxidized layer. The maximum concentration of metallic elements in oxides can be found at different depths of the oxidized layer. Starting from the surface of the oxide layer (formed during annealing of steel in a vacuum furnace with graphite heating chamber) the order of the oxidized metallic elements would be as follows: the highest values of Al, Ti, Cr, Mn, Fe and Ni (Fig. 12c,d). However, during annealing in a vacuum furnace with molybdenum heating chamber, the maximum concentration of oxidized metallic elements was different. Starting from the surface of the oxide layer the order of the elements would be as follows: Al, Cr, Mn, Fe, Ni and Ti. The similar results were achieved during the analysis of TEM with EDS chemical composition on cross-section of the thin foil of oxide layer formed in a vacuum furnace with molybdenum heating chamber. Taking into consideration the value of Gibbs free energy needed to create metal oxides, basing on the Ellingham-Richardson diagram [18], the Al, Ti, V, Mn, Cr, Fe and Ni oxides should be formed first.

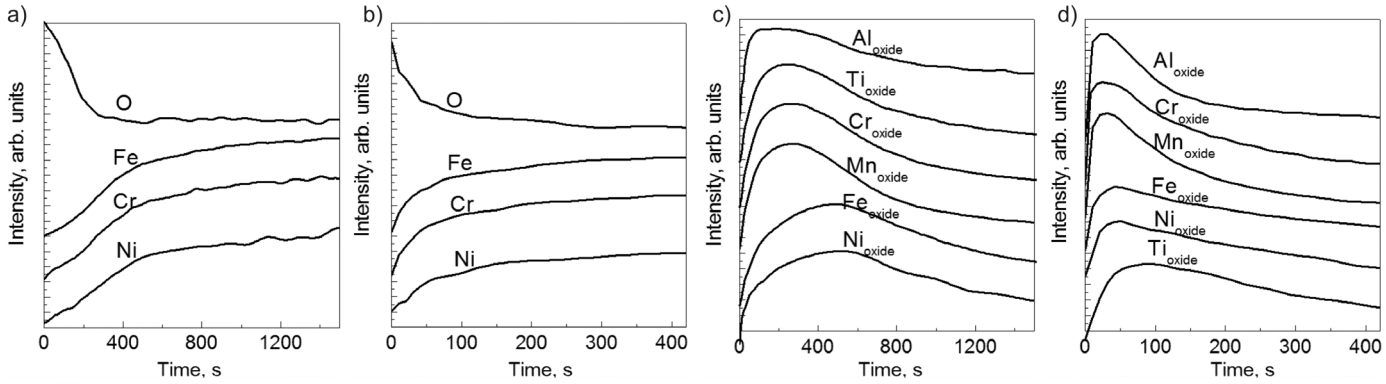

Fig. 12. TOF SIMS mass spectrum of the AISI 321 stainless steel: a) for elements after annealing in a vacuum furnace with graphite heating chamber, b) for elements after annealing in a vacuum furnace with molybdenum heating chamber, c) for oxidized metallic elements in a vacuum furnace with graphite heating chamber, d) for oxidized metallic elements in a vacuum furnace with molybdenum heating chamber

4. Conclusions

As a result of annealing of the AISI 321 steel, the formed oxide layer consisted of sub-layers differing form each other with chemical composition.

As a result of annealing of the AISI 321 steel at 980˚C in a ceramic furnace in oxidation atmosphere, the oxide layer, diversified in chemical composition, consisting mainly of Cr_2O_3 and Fe_3O_4 300-500 μm thick, is formed on the surface of steel.

The oxide layer formed in a vacuum furnace with molybdenum heating chamber, consists of smaller grains and has lower roughness in comparison to the grains of oxide layer formed in a vacuum furnace with graphite heating chamber. Little roughness of the surface and smaller length of oxide grain boundaries formed during annealing in a vacuum furnace with molybdenum heating chamber, influences the diffusion process of oxygen and metallic elements. It also affects the thickness of the oxide layer, which becomes smaller (up to 50 nm).

The thickness of the oxidized layer depends on the annealing conditions in a vacuum furnace. It is advisable (because of the thickness of the oxide layer) to anneal the AISI 321 stainless steel in a furnace with molybdenum heating chamber.

In oxide layers formed in vacuum furnaces there are no iron oxides.

Titanium, apart from being to link carbon in carbides, is a component of the oxide layer formed on the surface of the AISI 321 steel.

Acknowledgements

Financial support of Structural Funds in the Operational Program – Innovative Economy (IE OP) financed from the European Regional Development Fund – Project "Modern material technologies in aerospace industry", No. POIG.0101.02-00-015/08 is gratefully acknowledged.

REFERENCES

[1] F.M. McGuire, Stainless Steels for Design Engineers, ASM International, (2008).

[2] A.K. Roy, V. Virupaksha, Mat. Sci. Eng., A**452-453**, 665-672 (2007).

[3] P.J. Gellings, M.A. de Jongh, Corrosion Science **7**, 7, 413-416 (1967).

[4] L. Zhou, D.G. Arnell, D. Jahnson, A. Chew,. Journal of Materials Engineering and Performance **4**, 242-247 (1995).

[5] J. Kusiński, S. Kac, A. Kopia, A. Radziszewska, M. Rozmus-Górnikowska, B. Major, Ł. Major, J. Marczak, A. Lisiecki, Bulletin of the Polish Academy of Sciences Technical Sciences **60**, 4 (2012).

[6] Z.L. Li, H.Y. Zheng, K.M. Teh, Y.C. Liu, G.C. Lim, H.L. Seng, N.L. Yakovlev, Applied Surface Science **256**, 1582-1588 (2009).

[7] C.Y. Cui, X.G. Cui, X.D. Ren, M.J. Qi, J.D. Hu, Y.M. Wang, Applied Surface Science **305**, 817-824 (2014).

[8] P. Marshall, Austenitic Stainless Steels: Microstructure and Mechanical Properties, Elsevier Applied Science Publisher, (1984).

[9] A. Elrefaey, High-temperature brazing in aerospace engineering, In Woodhead Publishing Series in Welding and Other Joining Technologies, edited by M.C. Chaturvedi, Woodhead Publishing, Welding and Joining of Aerospace Materials, (2012).

[10] Č. Donik, A. Kocijan, D. Mandrino, I. Paulin, M. Jenko, B. Pihlar, Applied Surface Science **255**, 15, 7056-7061 (2009).

[11] S. Cissé, L. Laffont, B. Tanguy, M.C. Laffont, E. Andrieu, Corrosion Science **56**, 209-216 (2012).

[12] D.A. Harrington, A. Wieckowski, S.D. Rosasco, B.C. Schardt, G.N. Salaita, A.T. Hubbard, J.B. Lumsden, Corrosion Science **25**, 849-869 (1985).

[13] A.A. Abduluyahed, K.J. Kurzydłowski, Mater. Sci. Eng. A **256**, 34-38 (1998).

[14] T. Terachi, K. Fujii, K. Arioka, J. Nucl. Sci. Tech. **42**, 225-232 (2005).

[15] M. Salgado, A.C.S. Sabioni, A.M. Huntz; É.H. Rossi, Mat. Res. **11**, 2, 227-232 (2008).

[16] P. Stefanov, D. Stoychev, M. Stoycheva, A.R. Gonzalez-Elipe, Ts. Marinova, Surf. Interface Anal. **28**, 106-110 (1999).

[17] W. Zieliński, K.J. Kurzydłowski, Scripta Mater. **43**, 33-37 (2000).

[18] W.H. Freeman, J. Paula, Physical Chemistry: Thermodynamics And Kinetics, Oxford Univ. Press (2008).

Received: 20 April 2015.